

# RSC Advances



This is an *Accepted Manuscript*, which has been through the Royal Society of Chemistry peer review process and has been accepted for publication.

*Accepted Manuscripts* are published online shortly after acceptance, before technical editing, formatting and proof reading. Using this free service, authors can make their results available to the community, in citable form, before we publish the edited article. This *Accepted Manuscript* will be replaced by the edited, formatted and paginated article as soon as this is available.

You can find more information about *Accepted Manuscripts* in the [Information for Authors](#).

Please note that technical editing may introduce minor changes to the text and/or graphics, which may alter content. The journal's standard [Terms & Conditions](#) and the [Ethical guidelines](#) still apply. In no event shall the Royal Society of Chemistry be held responsible for any errors or omissions in this *Accepted Manuscript* or any consequences arising from the use of any information it contains.

# Synergetic effects of matrix crystalline structure and chain mobility on the low temperature toughness of polypropylene/ethylene-octene copolymer blends

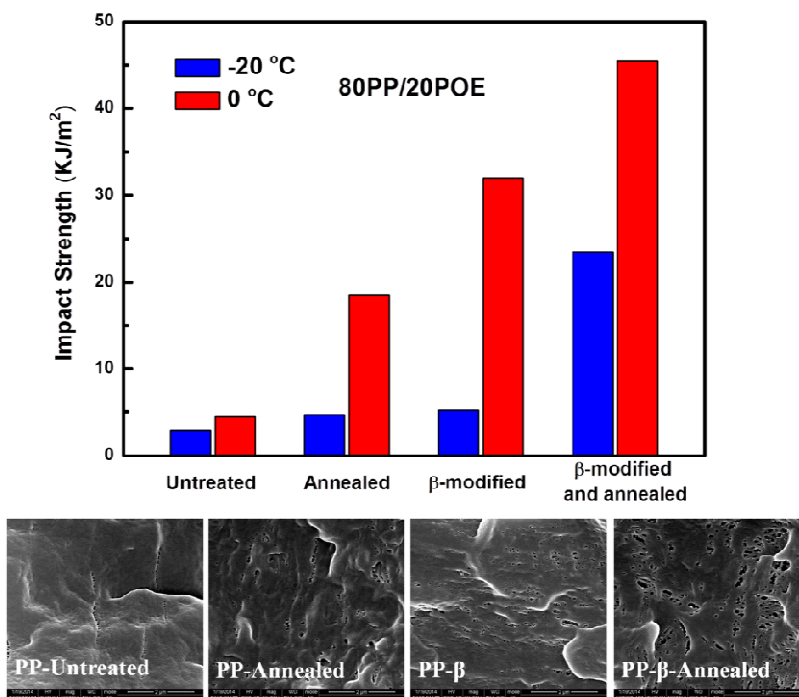
Xin Hu,<sup>a</sup> Chengzhen Geng,<sup>\*a,b</sup> Guanghui Yang,<sup>a</sup> Qiang Fu,<sup>\*a</sup>

Hongwei Bai<sup>a</sup>

<sup>a</sup> College of Polymer Science and Engineering, State Key Laboratory of Polymer Materials Engineering, Sichuan University, Chengdu, 610065, China.

<sup>b</sup> Institute of Chemical Materials, China Academy of Engineering Physics, Mianyang, 621900, China.

## Table of contents



Synergetic effects of matrix crystalline structure and chain mobility was investigated on the low temperature toughness of polypropylene/ethylene-octene copolymer blends.

**Synergetic effects of matrix crystalline structure and chain mobility on the low temperature toughness of polypropylene/ethylene-octene copolymer blends**

Xin Hu,<sup>a</sup> Chengzhen Geng,<sup>\*a,b</sup> Guanghui Yang,<sup>a</sup> Qiang Fu,<sup>\*a</sup>

Hongwei Bai<sup>a</sup>

<sup>a</sup> College of Polymer Science and Engineering, State Key Laboratory of Polymer Materials Engineering, Sichuan University, Chengdu, 610065, China.

<sup>b</sup> Institute of Chemical Materials, China Academy of Engineering Physics, Mianyang, 621900, China.

**\*Corresponding author:**

Qiang Fu:

E-mail: qiangfu@scu.edu.cn

Tel: +86-28-85461795

Fax: +86-28-85405402

Chengzhen Geng:

E-mail: zhenmail86@gmail.com

Tel: +86-816-2495514

Fax: +86-816-2495856

## Abstract

It is believed that the good toughness of  $\beta$ -modified polypropylene (PP) is due to its easier lamellar slippage compared with that of  $\alpha$ -modified PP, while the improvement in toughness of PP caused by annealing is due to increased chain mobility in amorphous part of PP. The aim of this work is to reveal the combined effects of matrix crystalline structure and amorphous chain mobility on the low temperature toughness of PP/ethylene-octene copolymer (POE) blends by  $\beta$ -modification and annealing. Impact test was performed over a wide range of temperatures (room temperature, 0 °C, -20 °C and -40 °C) to verify the enhancement in toughness, and various characterizations were carried out to inspect the structural evolutions and toughening mechanism. The results show that  $\beta$ -modification and annealing will work synergistically to toughen the blend and reduce the POE content necessary for effective toughening over the temperature range tested, due to the synergetic enhancement in matrix cavitation ability. Besides, the tensile properties will not be lowered by  $\beta$ -modification and annealing. This work not only paves a more efficient way to improving impact resistance of polymers with stiffness-toughness balance, but also demonstrates the vital role of matrix microstructures on toughness of the material.

**Key words:** low temperature toughness, stiffness-toughness balance,  $\beta$ -modification, annealing, cavitation.

## 1. Introduction

Owing to its rather versatile properties and low cost, polypropylene (PP) has become one of the most important polymers widely used in automobile, construction, pipe and domestic industries [1-5]. But its rather poor impact resistance strongly limits its wider application, especially at temperatures below its glass transition (around or below 0 °C) when its amorphous phase is frozen in the glassy state [5-11]. So much work has been carried out to improve the low temperature toughness of PP [7-11].

Up to now, blending with elastomers and copolymerization with minor olefins, in which elastomer dispersed phase would form in the PP amorphous phase through a phase separation process during crystallization, are the most efficient approaches to improve its low temperature toughness [7-14]. Despite the cost of stiffness and strength, the elastomer will improve the mobility of the PP amorphous phase, allowing for cavitation in the amorphous phase (inside the elastomer domains or at the elastomer/PP interface) and facilitating the shear yielding/plastic flow of the crystalline network, consequently dissipating much energy [5, 7, 8, 10-12]. So numerous investigations have been conducted on the toughening behavior of elastomers [5, 8, 10, 12, 15-18]. In addition to their content, the key influencing factors on the toughness are considered to be compatibility of the elastomer with the PP matrix and the glass transition temperature ( $T_g$ ) of the elastomer [8, 9, 15, 16]. The compatibility will determine the phase morphology, which strongly affects the cavitation behavior, and the  $T_g$  is responsible for the improvement in amorphous chain mobility. Incorporation of elastomers with good compatibility and low  $T_g$  (such as ethylene-octene copolymer, POE) will improve the low temperature toughness of PP by a order of magnitude as long as its loading is high enough [5, 8, 9, 15, 17].

On the other hand, however, less attention is paid to the effect of PP intrinsic microstructures on the low temperature toughness [19-24]. As introduced above and demonstrated by previous works [7, 12, 15, 23, 24], the toughening behavior is

primarily initiated in the PP amorphous phase and the energy could be much dissipated in the PP crystalline phase. This means the matrix structure/property in both the crystalline and amorphous phase should play a role equally crucial to the elastomers. But only a few publications [19-24] focusing on this are available. Van der Wal's and Loyens' publications [20, 21] proved in their respective systems that matrix molecular weight and crystallinity could somehow affect the toughness of the blends. Jiang's work [22] showed that the product of the yield stress and yield strain of the matrix may be a key factor. Previous works conducted by Wang's group and our group [3, 9, 11, 23-26] have also confirmed the important role that matrix crystalline form, crystalline morphology and amorphous chain mobility play on the toughness of PP. By controlling these matrix factors, the content of elastomers necessary for high toughness (at room temperature) could be lowered and the stiffness of the materials could be better retained [5, 9, 11, 24]. Nonetheless, none of the above works focused on the low temperature toughness, and it is still unclear how the above factors in the crystalline and amorphous phase would interact with each other to further influence the toughness.

So in this work, PP/POE blends are chosen to reveal the combined effects of matrix crystalline structure and amorphous chain mobility on the low temperature toughness of the blends. The matrix crystalline structure is tailored by changing the crystalline form from the monoclinic  $\alpha$ -form with the interlocking crosshatch structure to the trigonal  $\beta$ -form without crosshatch. The crystallographic symmetry of the  $\beta$ -crystalline form with three equivalent glide planes could offer a higher probability for crystals to slip [11, 23, 25-30]. The amorphous chain mobility could be adjusted by annealing at elevated temperatures (lower than its melting point) after the crystalline perfection and finer structure adjustment during annealing based on our recent results [23-25, 30, 31]. Not only will the interplay between crystalline structure and amorphous phase mobility be discussed, but also the toughness of the blends over a wide range of temperatures as well as their tensile properties will be investigated. This work will give a deeper understanding in the toughening mechanism at low temperatures, and meanwhile provide guidance for producing PP with

stiffness-toughness balance.

## 2. Experimental

### 2.1 Materials and sample preparation

Isotactic polypropylene (PP) T30s, with the melt flow index (MFI) of 2.3 g/10 min (200 °C, 2.16 kg) and density of 0.91 g/cm<sup>3</sup>, was supplied by CNPC Lanzhou Chemical Company, China. Ethylene-octene copolymer (POE) Engage 8150, with MFI of 0.5g/10min, density of 0.868g g/cm<sup>3</sup> and octene content of 25 wt%, was purchased from DuPont Dow Elastomers. The  $\beta$ -nucleating agent, marked WBG, was nicely supplied by Guangdong Winner Functional Materials Co. (Foshan, Guangdong, China). The composition of this rare earth nucleating agent is hetero-nuclear dimetal complexes of lanthanum and calcium containing some specific ligands [3].

The as-obtained PP, POE pellets and WBG powders were melt blended in a co-rotating twin screw extruder (TSSJ-25 co-rotating twin-screw extruder, China) with the screw speed of 120 rpm and set temperatures of 160-200 °C from hopper to die. The WBG content was 0.2 wt% and the POE contents were 0 wt%, 5 wt%, 10 wt%, 20 wt%, 30 wt% and 40 wt%, respectively. Then the blend pellets were injection-molded into standard specimens for testing, conducted on an injection-molding machine (PS40E5 ASE, Japan) at the processing temperature of 200 °C. For comparison, PP/POE blends without WBG were also prepared by identical processing conditions. For annealing experiment, the samples were placed in a vacuum oven set at 135 °C for 2 h, and then cooled down in ambient air. Prior to testing, the samples were conditioned at 23 °C and 50% relative humidity for 48 h.

The specimens are marked according to the POE content and the modification method. For instance, PP/POE-A means the annealed blends, and 20OE- $\beta$ -A stands for the blends with 20 wt% POE by both  $\beta$ -modification and annealing.

## 2.2 Characterization

### 2.2.1 Mechanical Test

The notched Izod impact strength of the specimens was measured with a VJ-40 Izod machine according to ASTM D256-04. Before impact test, the specimens were kept in a container at a certain set temperature (-40 °C, -20 °C, 0 °C and 23 °C) for 12 h, respectively, then they were immediately subjected to impact. Tensile tests were performed at room temperature (23 °C) using an SANS Universal tensile test machine controlled by a two-step program, according to the GB/T 1040-92 standard, which is, the moving speed of crosshead was 5.00 mm/min and 50.00 mm/min for modulus and tensile strength measurements, respectively. The average values of all the properties were obtained from at least five specimens.

Dynamic mechanical analysis (DMA) was carried out using a DMA Q800 machine (TA instruments, USA). The three-point-bend mode was used, and the heating program was set from -85 to 130 °C at a heating rate of 3 °C/min. The oscillatory strain and frequency are respectively set as 0.1% and 1 Hz.

### 2.2.2 Scanning Electron Microscope (SEM)

Scanning electron microscopy (SEM) observations were carried out to inspect the impact fractured surfaces, the rubber domain morphologies and necking zone of tensile-deformed samples. The rubber domain morphology was obtained by cryo-fracturing the samples both parallel and vertical to the flow direction in liquid nitrogen and then etching the fractured samples in xylene at 60 °C for 40 min. The necking zone of tensile-deformed samples was also produced by cryo-fracture along the deformation direction. The surfaces were coated with gold and inspected using an FEI Inspect F SEM instrument with an acceleration voltage of 20 kV.

### 2.2.3 Wide-Angle X-Ray Diffraction (WAXD)

A Philips X'Pert pro MPD apparatus with Ni-filtered Cu K $\alpha$  radiation (wave length is 0.154 nm) was used to acquire the WAXD spectra. The spectra were recorded in the diffraction angle range of 10 $^{\circ}$ -24 $^{\circ}$  at 40 kV and 40 mA with a scanning rate of 5 %/min. The overall crystallinity ( $X_c$ ) and relative amount of the  $\beta$ -form crystalline ( $K_{\beta}$ ) were calculated according to the following equations, respectively [19]:

$$X_c = \frac{\sum A_{cryst}}{\sum A_{cryst} + \sum A_{amorp}} \quad (1)$$

$$K_{\beta} = \frac{A_{\beta(300)}}{A_{\alpha(110)} + A_{\alpha(040)} + A_{\alpha(130)} + A_{\beta(300)}} \quad (2)$$

where  $A_{cryst}$  and  $A_{amorp}$  are the fitted areas of crystalline and amorphous region, respectively.  $A_{\beta(300)}$  is the area of the (300) reflection peak of  $\beta$ -form at  $2\theta = 16.1^{\circ}$ ;  $A_{\alpha(110)}$ ,  $A_{\alpha(040)}$  and  $A_{\alpha(130)}$  are the areas of the (110), (040), and (130) reflection peaks of  $\alpha$ -form, corresponding to  $2\theta = 14.1^{\circ}$ ,  $16.9^{\circ}$  and  $18.6^{\circ}$ , respectively.

#### 2.2.4 Differential Scanning Calorimetry (DSC)

DSC was performed on a Perkin-Elmer pyris-1 DSC (USA), which was calibrated with high-purity indium as standard. For each test, about 5 mg specimen was sealed in aluminum pan and heated from 30  $^{\circ}$ C to 200  $^{\circ}$ C at a heating rate of 10  $^{\circ}$ C/min in dry nitrogen atmosphere.

### 3. Results and Discussion

#### 3.1 Mechanical Properties

The impact properties of the samples at various temperatures are shown in Figure 1. At room temperature (Figure 1 (A)), the untreated blends present a typical brittle-to-ductile (B-D) transition behavior with the increase of POE content. The transition content, where is the sharp shift in failure mode from brittle fracture with poor impact toughness to ductile fracture with excellent impact toughness, is around 20wt% POE loading. To “fully” toughen PP, about 30 wt% POE is needed, and the

impact strength could be enhanced from 3.5 kJ/m<sup>2</sup> to as high as 48.4 kJ/m<sup>2</sup>. In comparison, neither the  $\beta$ -modified nor the annealed blends show a B-D transition behavior, the impact property just increases gradually with POE content, consistent with previous works [24, 32]. The impact strength of either  $\beta$ -modified or annealed blends is higher than that of its untreated counterpart. For instance, the impact strength of 10OE-A (34 kJ/m<sup>2</sup>) is about 5.8 times that of 10OE (5.9 kJ/m<sup>2</sup>). Comparing the effects of  $\beta$ -modification and annealing, their difference in the toughening effect at room temperature is minor. By a combination of  $\beta$ -modification and annealing, the impact strength could be further improved, indicating a synergetic effect of matrix crystalline structure and amorphous chain mobility. Even PP- $\beta$ -A without POE (12.1 kJ/m<sup>2</sup>) is obviously tougher than PP (3.5 kJ/m<sup>2</sup>). The impact strength of 10OE- $\beta$ -A is increased to 45.9 kJ/m<sup>2</sup>, 7.8 times that of 10OE and comparable to that of 30OE (48.4 kJ/m<sup>2</sup>).

At the low temperature of 0 °C around the T<sub>g</sub> of PP (Figure 1 (B)), all the samples show a B-D transition behavior. For the untreated blends, the transition POE loading is increased to 30 wt% because the amorphous phase mobility of PP is significantly restrained at this temperature. In contrast, the transition loading is only 20 wt% for all the modified blends, suggesting that the POE content necessary for enhanced toughness at this temperature could be lowered by the improvement of matrix crystalline structure and/or amorphous chain mobility. Comparing different samples at the same POE content of 20 wt%, the toughness sequence is 20OE (4.5 kJ/m<sup>2</sup>), 20OE-A (18.5 kJ/m<sup>2</sup>), 20OE- $\beta$  (32 kJ/m<sup>2</sup>) and 20OE- $\beta$ -A (45.5 kJ/m<sup>2</sup>) from brittle to tough. The impact strength of 20OE- $\beta$ -A is comparable to that of 30OE at room temperature (48.4 kJ/m<sup>2</sup>), about 10 times that of 20OE, 2.5 times that of 20OE-A and 1.4 times that of 20OE- $\beta$  at 0 °C. These results demonstrate that a synergetic effect of matrix crystalline structure and amorphous chain mobility exists not only at room temperature but also at this low temperature.

When the test temperature is further decreased to -20 °C (Figure 1(C)), the B-D transition content is increased by about 10 wt% for untreated blends, PP/POE-A and PP/POE- $\beta$ . But the B-D transition content for PP/POE- $\beta$ -A is still around 20 wt%. The

impact strength of 20OE- $\beta$ -A is 23.5 kJ/m<sup>2</sup>, about 5~8 times that of its counterparts (3~5 kJ/m<sup>2</sup>). At higher POE loadings, PP/POE- $\beta$ -A still presents the best toughness among all samples. At our lowest test temperature of -40 °C around the glass transition range of POE (Figure 1(D)), the impact toughness of all the samples are significantly suppressed, but the sequence in toughness among different treatment conditions is still similar to that at 0 °C. PP/POE- $\beta$ -A still shows the best toughening effect. Impact strength of 30OE- $\beta$ -A (16.5 kJ/m<sup>2</sup>) is much higher than that of 30OE- $\beta$  (7.2 kJ/m<sup>2</sup>), 30OE-A (6.4 kJ/m<sup>2</sup>) or 30OE (3.8 kJ/m<sup>2</sup>), and 40OE- $\beta$ -A could present superior toughness of about 51 kJ/m<sup>2</sup>, highest among all the samples (41.6 kJ/m<sup>2</sup>, 25 kJ/m<sup>2</sup> and 9.2 kJ/m<sup>2</sup> for 40OE- $\beta$ , 40OE-A and 40OE, respectively). Again, the impact properties of the blends at -20 °C and -40 °C further confirm the synergetic effect of matrix crystalline structure and amorphous chain mobility at low temperatures. This effect is favor of improving toughness at lower POE loadings, which may reduce the content of POE needed to toughen PP at a particular temperature at a lower cost of the strength and modulus.

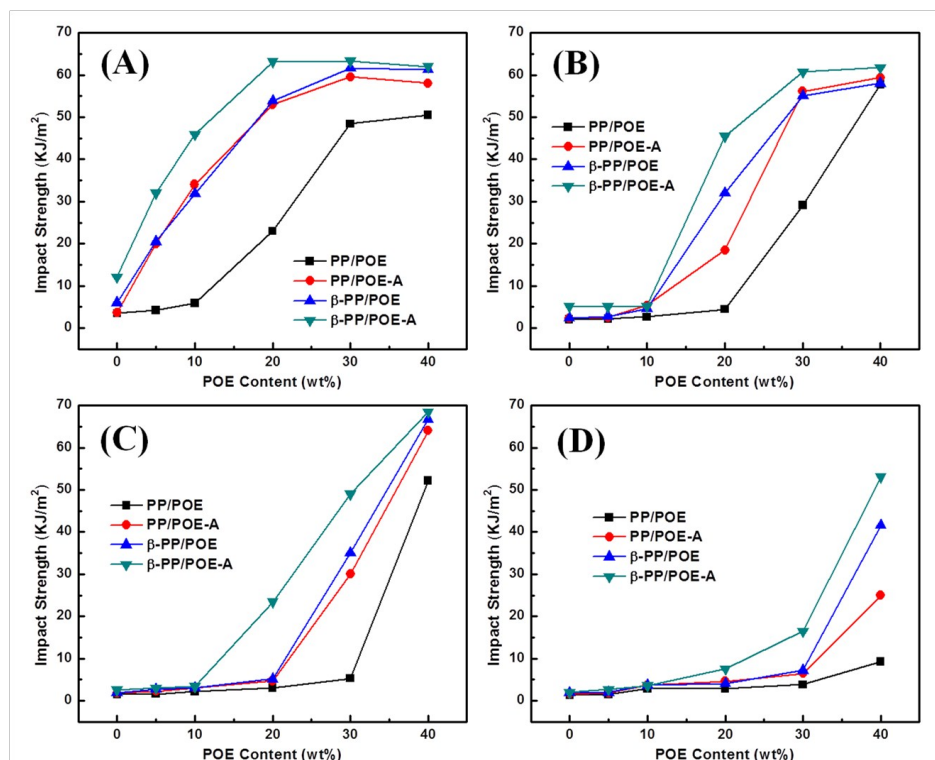


**Fig.1** effect of  $\beta$ -modification and annealing on the impact properties of PP/POE blends at various temperatures: (A) room temperature, (B) 0 °C, (C) -20 °C, (D) -40 °C.

The tensile properties of various samples are presented in Figure 2. From the typical stress-strain curves (Figure 2 (A,B)), it could be noticed that the untreated blends undergo a more intensive localized necking behavior with increasing strain, whereas less strain softening occurs for the modified samples, especially for PP/POE- $\beta$ -A. This suggests that  $\beta$ -modification and annealing synergistically suppresses the necking behavior of the blends and makes the material more favor of working as a whole to undergo deformation. Besides,  $\beta$ -modification and annealing also have an influence on elongation at break. Obviously,  $\beta$ -modification will improve the elongation at break to some degree as expected owing to the higher crystal slip ability of the  $\beta$ -form. But annealing will somehow decrease the elongation, in agreement with previous works [23, 31]. Interestingly, after a combination of  $\beta$ -modification and annealing, the elongation reverts to the level of untreated blends, indicating that the effects of  $\beta$ -modification and annealing on elongation somehow compromised each other in this case.

Figure 2 (C) and (D) show the Young's modulus and yield strength of various samples obtained from the stress-strain curves. Obviously, the addition of POE will decrease the modulus and strength of the material, so it is very important to lower the amount of POE. As for the effects of  $\beta$ -modification and annealing, they could also make some contributions to the modulus and strength. At the same POE loading,  $\beta$ -modification will decrease the strength and modulus of the material to some extent due to the lack of cross-hatch structure in the  $\beta$ -form, while annealing will somehow increase them owing to annealing-induced structural perfection and increase in crystallinity. Interestingly again, annealing-induced modulus/strength increase will roughly make up for the modulus/strength loss by  $\beta$ -modification in this system, so the strength and modulus of PP/POE- $\beta$ -A are very close to those of untreated PP/POE at the same POE loading. Combining the toughness results, PP/POE- $\beta$ -A offers not only the best low temperature toughness but also the best toughness-stiffness balance because the tensile properties are merely affected by a combination of  $\beta$ -modification and annealing, but the POE loading necessary for improved toughness could be

greatly reduced.

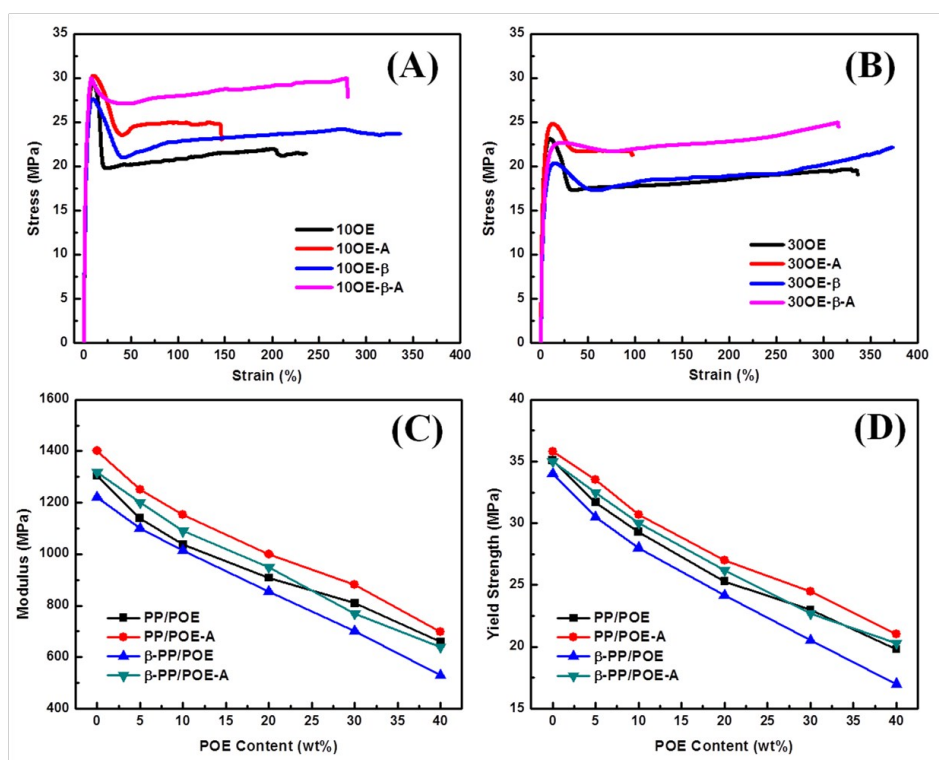


**Fig. 2** effect of  $\beta$ -modification and annealing on the tensile properties of PP/POE blends. (A) stress-strain curves of various blends with 10 wt% POE, (B) stress-strain curves of various blends with 30 wt% POE, (C) Young's Modulus of the samples, (D) yield strength of the samples.

### 3.2 Structure characterization

As is known, the dispersed phase in injection-molded parts usually shows an elongated morphology along the flow direction due to the shear field during processing [12, 33, 34]. In order to give an overall view of the phase morphologies, the samples are cryo-fractured along and vertical to the flow directions, respectively. Blends with 20 wt% and 40 wt% POE are taken as typical examples and their phase morphologies are shown in Figure 3. As is clearly seen in Figure 3 (A), (C), (E) and (G), there is scarcely any difference in phase morphology (size and morphology of POE droplets) among 20OE, 20OE-A, 20OE- $\beta$  and 20OE- $\beta$ -A in both directions, indicating that  $\beta$ -modification and annealing have no obvious influence on the phase morphology. As for the blends containing 40 wt% POE (Figure 3 (B), (D), (F) and

(H)), the phase morphology is about to transit from the “sea-island” morphology to the double-continuous morphology, but the phase morphologies of these blends still present no much difference.

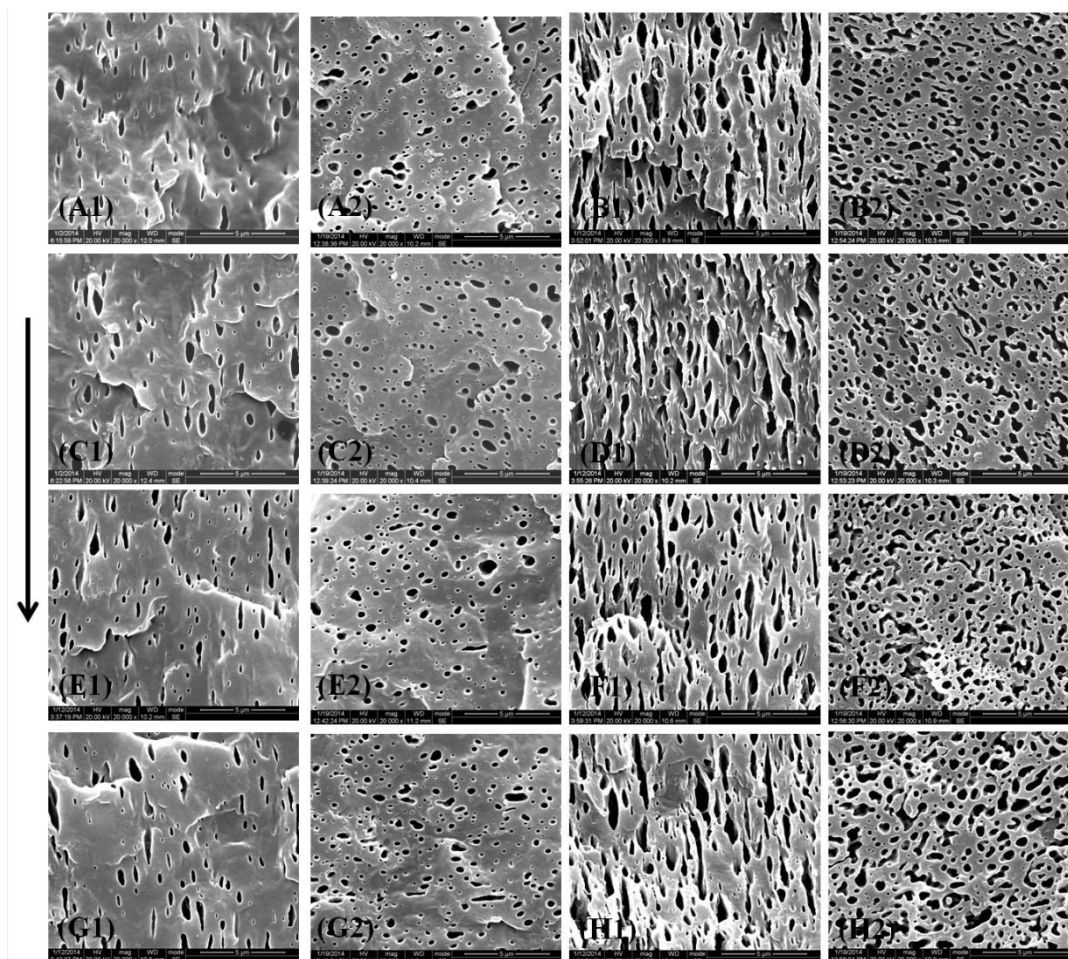


**Fig. 3** phase morphologies of (A) 20OE, (B) 40OE, (C) 20OE-A, (D) 40OE-A, (E) 20OE- $\beta$ , (F) 40OE- $\beta$ , (G) 20OE- $\beta$ -A, (H) 40OE- $\beta$ -A. The numbers 1 and 2 represents the samples are fractured along and vertical to the flow direction, respectively. The black arrow on the left indicates the flow direction of the parallel-fractured samples.

The WAXD profiles of various blends are illustrated in Figure 4 (taking blends with 20 wt% POE as a typical example) and the data calculated from the profiles according to Equation 1 and 2 are listed in Table 1. Firstly,  $\beta$ -nucleating agent has a strong influence on the crystalline form as expected. With the addition of 0.2 wt% nucleating agent,  $K_{\beta}$  is increased from 0 to 0.84 for unannealed samples, which

confirms its strong selective nucleating efficiency and thus the improvement in crystalline slippage by  $\beta$ -modification. The addition of  $\beta$ -nucleating agent also increases the crystallinity to a small degree (by 0.01-0.02) owing to its nucleating effectiveness. Secondly, annealing has a minor effect on the crystallinity and crystalline form composition. After annealing, there is a small increase in  $X_c$  (by 1-2%) due to crystalline perfection or formation of new crystals, and a slight decrease in  $K_\beta$  (by 5%) due to the  $\beta$ -to- $\alpha$  transition during annealing. These results agree well with previous works [11, 23, 25], and also correlate well with the change in strength and modulus after  $\beta$ -modification and annealing.

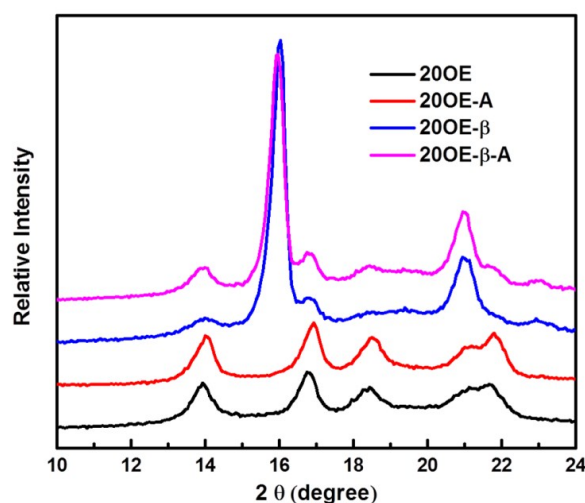


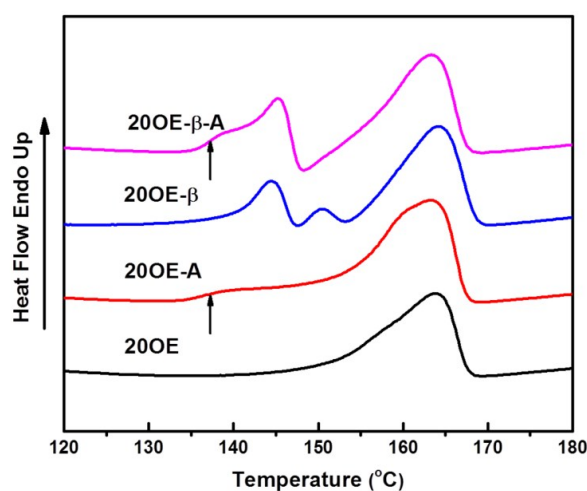
Fig. 4 WAXD profiles of the samples treated under various conditions.

Table 1  $X_c$ ,  $K_\beta$  and  $T_g$  of PP for various samples obtained from WAXD and DSC

	20OE	20OE-A	20OE- $\beta$	20OE- $\beta$ -A
$X_c$	0.52	0.53	0.55	0.57
$K_\beta$	0	0	0.84	0.79
$T_g$ ( $^{\circ}C$ )	20	17	20	17

DSC melting curves of various samples are exhibited in Figure 5 (taking blends with 20 wt% POE as a typical example). Compared to that of 20OE, the thermogram of 20OE- $\beta$  shows a multiple-melting behavior. There are three main endothermic

peaks in its thermogram, which are  $\beta_1$ ,  $\beta_2$  and  $\alpha$  melting peak from low to high temperature. The two melting peaks at lower temperature range correspond to the melting of  $\beta$ -form PP, in which endotherm  $\beta_1$  is considered the melting of originally-formed  $\beta$ -PP, whereas melting peak  $\beta_2$  is related to the fusion of perfected/thickened lamellae formed by partial melting and recrystallization of initially-formed crystals upon DSC heating program [35, 36]. On the other hand, annealing also has a prominent influence on the melting behavior of the samples. As indicated by the black arrows, both annealed blends show a shoulder peak called “annealing peak” at around 138 °C compared to their unannealed counterparts. In previous works [23-25, 31, 35], the appearance of annealing peak is explained to be the result of thickening of existing crystals, new crystal formation, or relaxation of the confined rigid amorphous phase coupling to crystals during annealing. These microstructure evolutions are considered to be closely connected to the improvement in mobility of the amorphous phase [23-25, 31, 35]. In addition, for 20OE- $\beta$ -A, the  $\beta_2$  melting peak disappears. This could be explained by the perfection/thickening of the originally-formed  $\beta$  crystals during annealing [35].



**Fig. 5** DSC heating curves of the samples treated under various conditions.

Figure 6 shows plots of the mechanical loss factor ( $\tan \delta$ ) as a function of temperature for various blends (taking blends with 20 wt% POE as a typical example),

and glass transition temperatures ( $T_g$ ) of PP in different samples obtained from the plots are listed in Table 1. Three pronounced loss peaks can be observed in the plots. The first maxima at about  $-38\text{ }^\circ\text{C}$  is associated with the glass transition of POE, the second peak at around  $20\text{ }^\circ\text{C}$  is related to the glass transition of PP, and the third maximum at higher temperature range is associated with the  $\alpha$ -relaxation of PP originated from intra-lamellar block-slip process in the crystalline phase or segment diffusion at the interface of the crystalline/amorphous phase (or confined rigid amorphous phase) [23-25, 31, 35]. As is clearly seen, the relaxation behavior of POE shows no much difference among these samples, indicating that  $\beta$ -modification and annealing would not influence the POE phase obviously. On the other hand,  $\beta$ -modification does not affect the relaxation behavior of the PP phase, either. But annealing seems to exhibit a notable effect. After annealing,  $T_g$  of PP is decreased by about  $3\text{ }^\circ\text{C}$  for both untreated and  $\beta$ -modified blends, and the  $\alpha$  relaxation temperature also presents a notable increase trend. The  $\alpha$ -relaxation temperature is increased because of crystalline perfection or improved crystalline-amorphous interface after annealing, while the decrease in  $T_g$  confirms the improvement in mobility of the amorphous phase, and could be a result of the decreased chain density in the amorphous phase after annealing [23-25, 31, 35]. As is discussed above, the structure changes after annealing may include lamella perfection, thickening of the crystalline lamellas and increase in crystallinity, which suggests that a portion of the amorphous segments are rearranged into the crystalline phase during annealing, and thus the number of segments in the amorphous phase is decreased. Furthermore, our recent investigations demonstrated that the thickness of PP amorphous phase between lamellas would increase after annealing, in spite of the crystalline form [31, 35], further verifying that the chain density in the amorphous phase will decrease after annealing. As a result, the mobility of the amorphous segments is enhanced and  $T_g$  is lowered.

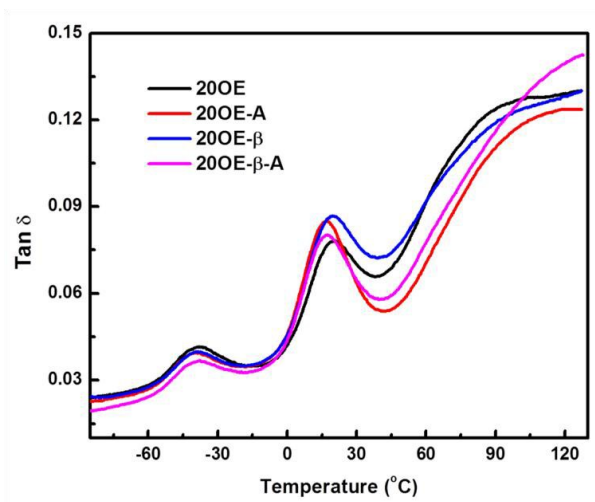


**Fig. 6** mechanical loss factor of various blends as a function of temperature.

### 3.3 Toughening Mechanism

To investigate the synergistically toughening mechanism of matrix crystalline structure and amorphous chain mobility, SEM is adopted to inspect the impact-fractured surfaces of the samples. Typical micrographs of impact-fractured surfaces are shown in Figure 7. For either 20OE fractured at  $-20\text{ }^{\circ}\text{C}$  or 40OE fractured at  $-40\text{ }^{\circ}\text{C}$ , the untreated blends show a relatively smooth fractured surface, suggesting rapid fracture of the material and a brittle fracture mode. After annealing, more obvious plastic deformation (rougher surface) could be noticed, which will dissipate more energy and make the material tougher [15, 16, 23, 31, 32, 35]. As for the  $\beta$ -modified samples, the extent of plastic deformation is more severe, which is consistent with their higher toughness. However, it is difficult to distinguish the difference in extent of plastic deformation between PP/POE- $\beta$  and PP/POE- $\beta$ -A at the scale in Figure 7.

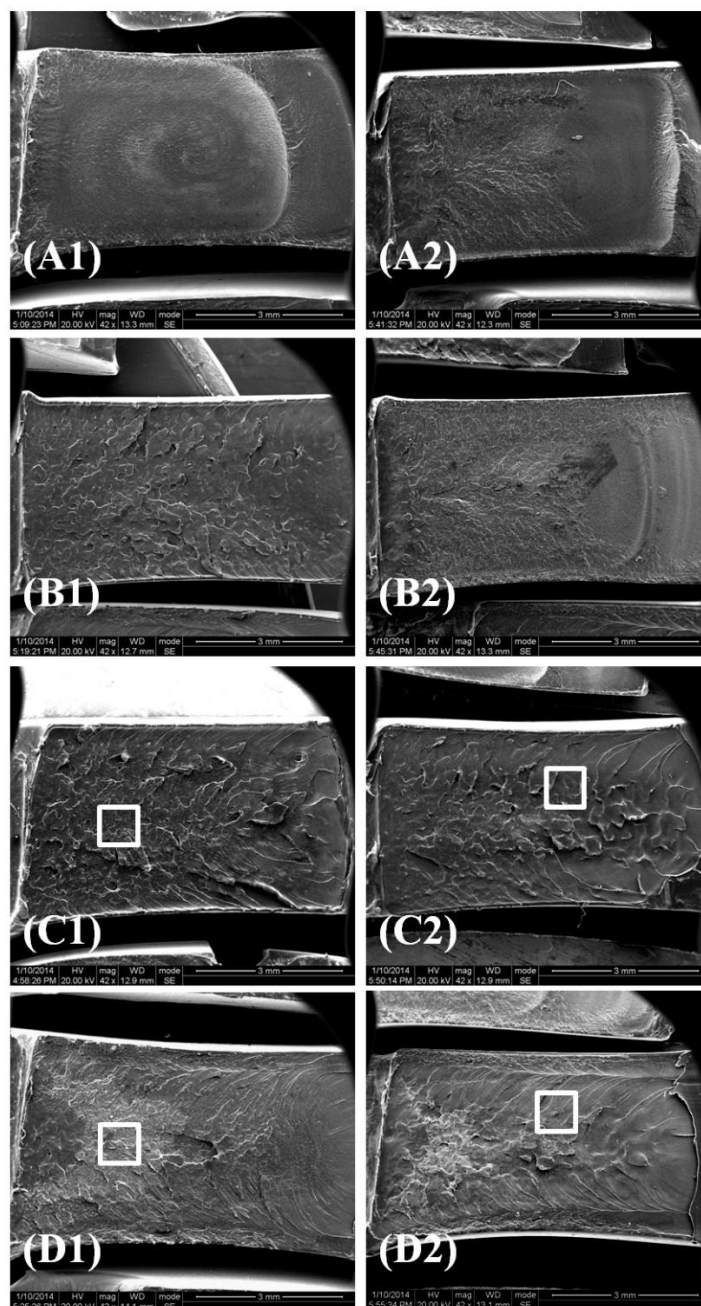


**Fig. 7** impact fractured surfaces of various samples: (A) PP/POE, (B) PP/POE-A, (C)  $\beta$ -PP/POE, (D)  $\beta$ -PP/POE-A. The numbers 1 and 2 represent 20wt% POE blends fractured at 0 °C and 40 wt% POE blends fractured at -40 °C, respectively. The white squares are indicators for Fig. 8.

Some typical regions (whitened zones) in the SEM micrographs of PP/POE- $\beta$  and PP/POE- $\beta$ -A are magnified and the micrographs are exhibited in Figure 8. As is clearly seen, the brighter zone on the fractured surfaces of PP/POE- $\beta$ -A present a high extent of plastic deformation with fibril morphologies pulled out, the formation of which may dissipate much energy [3]. In contrast, the morphology for PP/POE- $\beta$  at

the corresponding region shows a rather smooth morphology at this scale. Besides, the position out of the brighter zone shows a lot of striations (sheet-like sheared fragments) perpendicular to the crack propagation direction for PP/POE- $\beta$ -A, which is also strongly related to large local deformations and high strain energy dissipation [31], while its counterpart without annealing still shows a rather smooth morphology. So PP/POE- $\beta$ -A is much more severe than PP/POE- $\beta$  in the extent of plastic deformation.

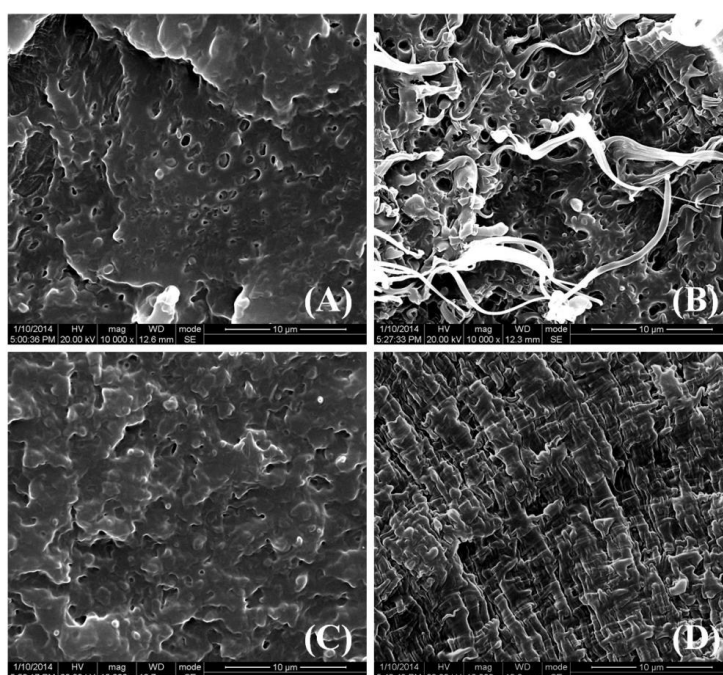


**Fig. 8** enlarged SEM figures of the white-squared areas in Fig. 7. (A) for Fig. 7 (C1), (B) for Fig. 7 (D1), (C) for Fig. 7 (C2), (D) for Fig 7. (D2).

Combining the above observations, the extent of plastic deformation is in the sequence of PP/POE, PP/POE-A, PP/POE- $\beta$  and PP/POE- $\beta$ -A, which agree very well with their sequence in toughness and the synergistically toughening effect of matrix crystalline structure and amorphous chain mobility. It is well known that toughening of PP is strongly related to its plastic deformation behavior [19, 31, 32, 35], so it is clear that the different extents of plastic deformation will account for their toughness variation. But it is still not lucid whether the improvement in plastic deformation

ability is directly originated from the improvement in matrix crystalline structure and amorphous chain mobility. As is generally accepted [31, 32, 35, 37], micro-voids play a crucial role in initiating plastic flow of the PP matrix. So necking zone of tensile deformed samples are observed using SEM to inspect the cavitation ability of different samples, as shown in Figure 9.

For PP (Figure 9(A1-D1)), samples with various modifications show a significant difference in cavitation ability. Few micro-voids could be observed in untreated PP, but more micro-voids would form during deformation after annealing. For PP- $\beta$ , its cavitation ability is higher than PP-A (higher density of micro-voids), and PP- $\beta$ -A shows the highest cavitation ability. The sequence in the cavitation ability of various PP samples correlates well with their degree of plastic deformation as well as their toughness. The results on cavitation ability could prove a synergetic effect of matrix crystalline structure and amorphous chain mobility on the cavitation ability of PP. As is known, the  $\beta$ -form PP has no cross-hatch structure between lamellas, so its crystal slip ability is higher, which will result in higher cavitation ability in the amorphous phase and easier shear yielding of the crystalline phase [4, 7, 11, 32, 38]. After annealing, the mobility in the amorphous is improved with the segmental density decreased as discussed above, which will also lead to easier cavitation in the amorphous phase. The above results and discussions manifest that these two effects in the crystalline and amorphous phase could work together to enhance the cavitation ability, promote the shear yielding/plastic flow of the crystalline phase and thus improve the toughness synergistically.

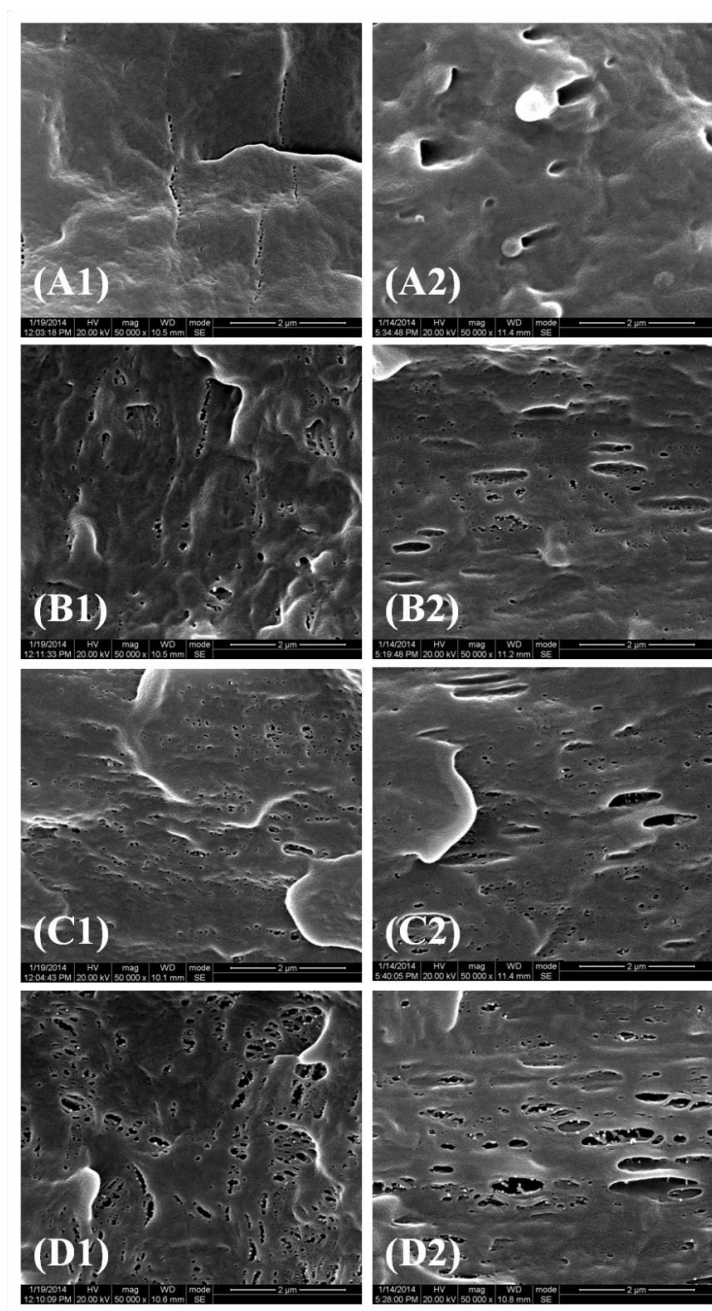


**Fig. 9** SEM micrographs of the necking zone of various samples (A) untreated samples, (B) annealed samples, (C) $\beta$ -nucleated samples, (D) $\beta$ -nucleated and annealed samples. The numbers 1 and 2 represent PP and PP/20wt% POE blends, respectively.

For the PP/POE blends (Figure 9 (A2-D2)), cavitation behavior is easier to occur within the elastomer phase or at the PP-POE interface [12]. So much larger micro-voids could be found in all the blends due to the existence of elastomers. But it is noteworthy that there are also some much smaller voids in the annealed or  $\beta$ -modified blends, the sizes of which are comparable to those in their PP counterparts.

It is reasonable to believe that these smaller voids are originated from the matrix. This means the higher cavitation ability of the matrix may also strongly affect the cavitation ability of the blends, resulting in a higher plastic deformation ability of the material. Considering that the phase morphology and relaxation behavior of the POE phase do not change notably by  $\beta$ -modification and annealing, the toughening mechanism directly contributed by POE should not be improved so significantly. So it is reasonable to infer that the modifications in the matrix structure are the main reason for the toughness enhancement. After  $\beta$ -modification and/or annealing, the enhancement in matrix crystalline structure and amorphous chain mobility could lead to easier cavitation in the amorphous phase and possibly more available shear yielding of the crystalline phase, which could work synergistically with each other to improve the toughness of PP/POE blends at various temperatures.

What's more, it is also noteworthy that the synergetic role of matrix crystalline structure and amorphous chain mobility is much more pronounced in PP/POE blends than in pure PP, especially at low temperatures below the  $T_g$  of PP (Figure 1). This is acceptable because the POE phase offers additional mobility in the amorphous phase. At a low temperature when the amorphous phase is frozen, the toughening effects of matrix crystalline structure and amorphous chain mobility would not work without the assistance of the POE phase. In order to design and prepare PP with superior toughness or toughness-stiffness balance, matrix structures/properties (including the crystalline phase and the amorphous phase) and the elastomer phase should be equally considered and tailored.

#### 4. Conclusion

Annealing and  $\beta$ -modification could enhance the matrix amorphous chain mobility and lamellar slippage, respectively. Not only could they improve the toughness of PP/POE blends and lower the POE content necessary for effective toughening, but also they present a synergetic effect to further toughen the blends over a wide range of low temperatures. It is inferred that the change in matrix

crystalline structure and enhancement in amorphous chain mobility could synergistically improve the cavitation ability of the PP matrix, facilitating more severe plastic flow and thus toughen the material with the assistance of the POE phase. This work not only provides a new and efficient approach to improve the low temperature toughness of PP and meanwhile retain its stiffness, but also reveals the synergetic contribution of the matrix microstructures on fracture resistance of the material.

## Acknowledgement

This work was supported by the National Natural Science Foundation of China (grant no. 51421061 and grant no. 21404075).

## References

- [1] F. Ghaemi, R. Yunus, M. A. M. Salleh, S. A. Rashid, A. Ahmadian and H. N. Lim, *RSC Adv.*, 2015, **5**, 28822-28831.
- [2] R. P. Ramasamy, K. Yang and M. H. Rafailovich, *RSC Adv.*, 2014, **4**, 44888-44895.
- [3] F. Luo, C. Geng, K. Wang, H. Deng, F. Chen, Q. Fu and N. Bing, *Macromolecules*, 2009, **42**, 9325–9331.
- [4] T. Wu, M. Xiang, Y. Cao, J. Kang and F. Yang, *RSC Adv.*, 2014, **4**, 43012-43023.
- [5] H. Du, Y. Zhang, H. Liu, K. Liu, M. Jin, X. Li and J. Zhang, *Polymer*, 2014, **55**, 5001-5012.
- [6] C.-M. Chan, J. Wu, J.-X. Li and Y.-K. Cheung, *Polymer*, 2002, **43**, 2981-2992.
- [7] C. Grein, C. J. G Plummer, H.-H. Kausch, Y. Germain and Ph. Béguelin, *Polymer*, 2002, **43**, 3279-3293.
- [8] J. Wang, C. Wang, X. Zhang, H. Wu and S. Guo, *RSC Adv.*, 2014, **4**, 20297-20307.
- [9] F. Luo, C. Xu, K. Wang, H. Deng, F. Chen and Q. Fu, *Polymer*, 2012, **53**, 1783-1790.
- [10] T. McNally, P. McShane, G. M. Nally, W. R. Murphy, M. Cook and A. Miller, *Polymer*, 2002, **43**, 3785-3793.

- [11] F. Luo, J. Wang, H. Bai, K. Wang, H. Deng, Q. Zhang, F. Chen, Q. Fu and B. Na, *Mater. Sci. Eng.: A*, 2011, **528**, 7052–7059.
- [12] C. Geng, J. Su, S. Han, K. Wang, and Q. Fu, *Polymer*, 2013, **54**, 3392-3401.
- [13] H. Zhu, B. Monrabal, C. C. Han and D. Wang, *Macromolecules*, 2008, **41**, 826-833.
- [14] J. Wang, H. Niu, J. Dong, J. Du and C. C. Han, *Polymer*, 2012, **53**, 1507-1516.
- [15] R. R. Tiwari and D. R. Paul, *Polymer*, 2011, **52**, 5595-5605.
- [16] F. Chen, B. Qiu, B. Wang, Y. Shangguan and Q. Zheng, *RSC Adv.*, 2015, **5**, 20831-20837.
- [17] C. Li, S. Yang, J. Wang, J. Guo, H. Wu and S. Guo, *RSC Adv.*, 2014, **4**, 55119-55132.
- [18] R. R. Tiwari and D. R. Paul, *Polymer*, 2011, **52**, 4955-4569.
- [19] T. Bárány, T. Czigány and J. Karger-Kocsis, *Prog. Polym. Sci.*, 2010, **35**, 1257–1287.
- [20] A. van der Wal, J. J. Mulder, J. Oderkerk and R. J. Gaymans, *Polymer*, 1998, **39**, 6781-6787.
- [21] W. Loyens and G. Groeninckx, *Polymer*, 2003, **44**, 123-136.
- [22] W. Jiang, D. Yu and B. Jiang, *Polymer*, 2004, **45**, 6437-6430.
- [23] H. Bai, Y. Wang, Z. Zhang, L. Han, Y. Li, L. Liu, Z. Zhou and Y. Men, *Macromolecules*, 2009, **42**, 6647-6655.
- [24] H. Wu, X. Li, Y. H. Wang, J. Wu, T. Huang and Y. Wang, *Mater. Sci. Eng.: A*, 2011, **528**, 8013-8020.
- [25] C. Geng, J. Su, C. Zhou, H. Bai, G. Yang and Q. Fu, *Compos. Sci. Technol.*, 2014, **96**, 56-62.
- [26] X. Li, H. Wu, L. Han, T. Huang, Y. Wang, H. Bai, Z. Zhou, *J. Polym. Sci. Part B: Polym. Phys.*, 2010, **48**, 2108–2120.
- [27] G. Coulon, G. Castelein and C. G'ssell, *Polymer*, 1999, **40**, 95-110.
- [28] J. Varga, *J. Macromol. Sci. B*, 2002, **41**, 1121-1171.
- [29] T. Wu, M. Xiang, Y. Cao, J. Kang and F. Yang, *RSC Adv.*, 2014, **4**, 36689-36701.
- [30] X.-W. Wang, J. Dai, J.-W. Chen, J. Duan, J.-H. Yang, J.-H. Zhang and Y. Wang,

*Ind. Eng. Chem. Res.*, 2015, **54**, 4976-4987.

[31] C. Geng, G. Yang, H. Bai, Y. Li, Q. Fu and H. Deng, *J. Supercrit. Fluid*, 2014, **87**, 83-92.

[32] H. Bai, Y. Wang, B. Song and L. Han, *J. Appl. Polym. Sci.*, 2008, **108**, 3270-3280.

[33] C.-Z. Geng, Y.-L. Zhu, G.-H. Yang, Q. Fu, C.-L. Zhang, K. Wang and T.-N. Zhou, *Chinese J. Polym. Sci.*, 2014, **32**, 9-20.

[34] Y.-H. Li, M. Zhou, C.-Z. Geng, F. Chen and Q. Fu, *Chinese J. Polym. Sci.*, 2014, **32**, 1724-1736.

[35] H. Bai, F. Luo, T. Zhou, H. Deng, K. Wang and Q. Fu, *Polymer*, 2011, **52**, 2351-2360.

[36] J. Karger-Kocsis and P. Shang, *J. Therm. Anal.*, 1998, **51**, 237-244.

[37] B. Na and R. Lv, *J. Appl. Polym. Sci.*, 2007, **105**, 3274-3279.

[38] T. Wu, M. Xiang, Y. Cao, J. Kang and F. Yang, *RSC Adv.*, 2015, **5**, 43496-43507.